A Nature Portfolio journal



https://doi.org/10.1038/s43247-025-02783-3

Subglacial geology and palaeo flow of Pine Island Glacier from combining glacial erratics with geophysics

Check for updates

Tom A. Jordan ®¹⊠, Joanne S. Johnson ®¹, Teal R. Riley ®¹, Ethan Conrad² & Andrew Carter ®²³

Subglacial geology plays a key role in determining the rate of ice flow and sensitivity of the glacial system to atmospheric or ocean warming. However, bedrock geology is often poorly known because direct information from subglacial samples is extremely challenging to obtain. Here, we combine the distribution, petrology, crystallisation age and thermochronology of glacial erratics with geophysical analyses to provide evidence for Middle Jurassic (~175 Ma) granitic bedrock extending beneath Pine Island Glacier, West Antarctica. Our results constrain the range of past ice flow pathways across the adjacent Hudson Mountains, providing information needed to improve models of ice sheet evolution in this vulnerable region. This work demonstrates the utility of integrating erratic geochemistry, geochronology and aerogeophysics for the study of subglacial environments and confirms erratics as a valuable, but largely untapped, source of evidence for what lies beneath the world's ice sheets.

The subglacial environment of Antarctica is both challenging and very costly to access, making the ice sheet bed one of the remotest and least well-known parts of Earth. However, knowledge of subglacial geology is critical for understanding processes that impact ice sheet flow, such as basal sliding and water flow¹⁻³. Thus, model projections of future ice sheet change in response to climatic warming (such as the rate of ice sheet mass loss) will be more reliable when the subglacial geology of Antarctica is better constrained. Without access to extensive subglacial drilling, two other distinct but complementary methods can be used to deduce subglacial geology: (1) geophysical surveys which reveal the spatial pattern of subglacial geological structures², but retain large ambiguities about lithology, and (2) examination of glacially transported rock and sediments, which can directly reveal subglacial lithology, but not its precise location due to uncertainty in the location of erosion and ice transport pathways⁴. Here, we combine both methodologies to provide fresh insights into the geology of the bed underlying Pine Island Glacier (PIG). Improving our understanding of this region of West Antarctica (Fig. 1a) is critical due to its ongoing and dominant contribution to sea level rise from the Antarctic Ice Sheet⁵.

Glacial erratics (cobbles and boulders transported by ice and exposed during subsequent ice sheet retreat) are numerous around the Antarctic continent and, because they originated as bedrock plucked by the overriding ice sheet during subglacial erosion, offer a direct window into what lies beneath the ice sheet. Samples of >3500 erratics have been collected from around Antarctica⁶ (Supplementary Fig. S1), but most have only been utilised to determine ice surface elevation changes via surface exposure

dating (e.g.⁷). These samples therefore represent a large and mostly untapped resource for studying the Antarctic subglacial environment. While ice-rafted debris found in marine sediments also provides evidence of subglacial geology, in contrast to erratics, marine material is typically recovered as a disaggregated sediment fraction rather than macroscopic samples. Thus, analysis of such ice-rafted debris is associated with a higher level of uncertainty as to the precise lithology of its original source rock.

Provenance methods have been applied around Antarctica to determine the source of ice-rafted debris and origin of tills and moraines on inland nunataks⁹. These applications have largely focused on the Ross Sea region^{10–13}, with a few in the Weddell Sea sector^{4,14} and around the margins of East Antarctica^{15,16} and the Amundsen Sea^{17,18}. A study focused on the PIG region determined the provenance of detrital grains in seafloor sediments⁸, showing differences in age and geochemistry between PIG and Thwaites Glacier catchments. However, no studies have used glacial erratics to directly investigate the subglacial geology and specific lithologies beneath the PIG catchment, as has been done in East Antarctica¹⁹.

In this study, we integrate the petrography, spatial distribution, U-Pb crystallisation ages and thermochronology (uplift and cooling history) of a suite of erratics with airborne geophysical maps and modelling to infer the subglacial geology and former ice flow paths in the PIG region of Antarctica. The 12 erratic cobbles and boulders (Supplementary Fig. S2) from the Hudson Mountains, situated adjacent to PIG in the eastern Amundsen Sea sector (Fig. 1b), were originally collected for ¹⁰Be exposure dating. These rocks were all glacially transported to the Hudson Mountains and stranded on the peaks when the West Antarctic Ice Sheet retreated after the last glacial

¹British Antarctic Survey, Cambridge, UK. ²Department of Earth Sciences, London Geochronology Centre, University College London, London, UK. ³School of Natural Sciences, Birkbeck, University of London, London, UK. e-mail: tomj@bas.ac.uk

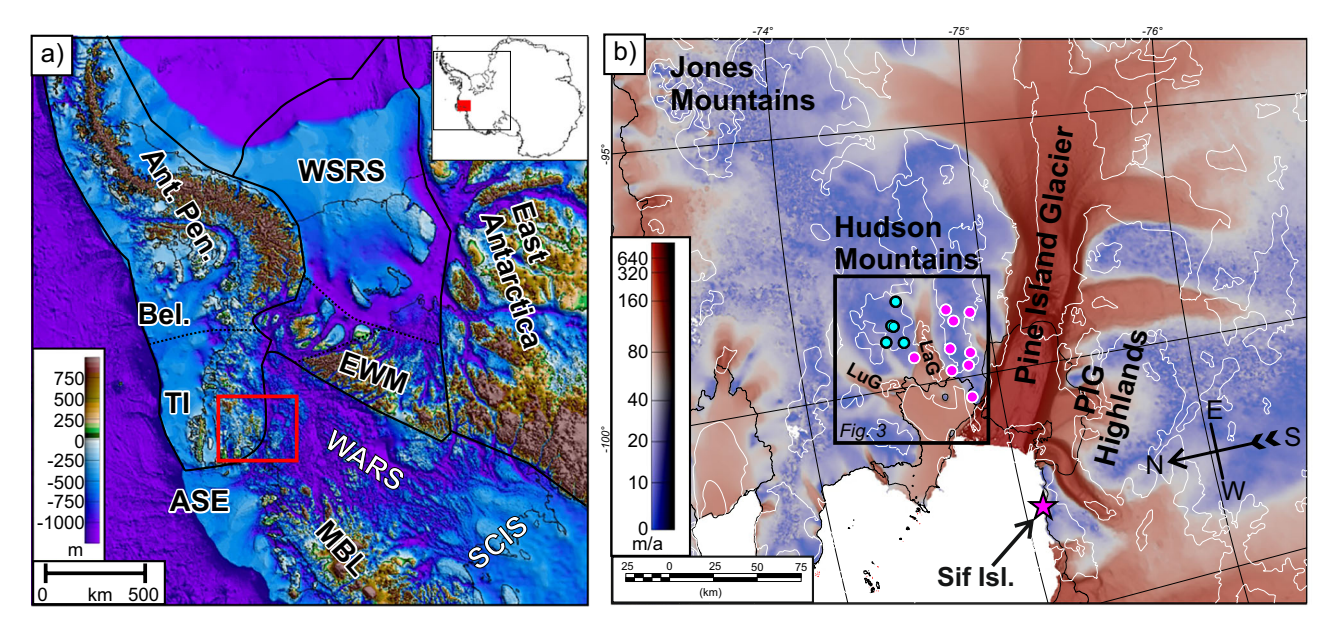


Fig. 1 | Study area overview. a Subglacial topography of West Antarctica⁶⁸. Black lines locate geological province boundaries⁷⁹. The inset locates study in Antarctica. The red box shows study area in (b). Ant. Pen. Antarctic Peninsula, WSRS Weddell Sea Rift System, Bel. Bellingshausen Sea, EWM Ellsworth-Whitmore Mountains, TI Thurston Island, ASE Amundsen Sea Embayment, WARS West Antarctic Rift System, SCIS Siple Coast Ice Streams, MBL Marie Byrd Land. b Ice velocity over the

Hudson Mountains and adjacent Pine Island Glacier (PIG)⁷⁴. White lines show 500 m contours of bed elevation. Pink star locates exposed pink granite basement²⁶. Pink dots represent locations of pink granite erratics in the Hudson Mountains; blue dots locate areas where erratics are present but are not composed of pink granite. Black box locates Fig. 3a. LaG Larter Glacier, LuG Lucchitta Glacier.

maximum (LGM)²⁰⁻²². They therefore provide key insights into the sub-glacial geology of the area that are unavailable from outcropping rocks.

Results

Field observations

The outcropping bedrock of the Hudson Mountains is composed entirely of basaltic lavas and hydrovolcanic rocks (hyaloclastites and tuffs) erupted between 3 and 8 Ma²³. Numerous glacial erratic cobbles and boulders of exotic lithology (predominantly syenite, alkali granite, granodiorite and tonalite) are perched on the scoured bedrock surfaces or resting on fragmented lava regolith²⁴ (Fig. 2a, Supplementary Fig. S2 and Supplementary Table S1). Bedrock striations, produced when thick (erosive) ice flows over rock, are rare and restricted to relatively small areas of outcrop, but were found at seven locations. Where present, field measurements of striated bedrock surfaces generally indicate flow in a N-S direction with a minor grouping suggesting NW-SE-oriented flow ²⁴ (Fig. 3a).

Field surveys demonstrate that pink granitoids – of syenite and alkali granite composition – are particularly common amongst the erratics in the area²⁴, with seven of the twelve erratics analysed in this study formed of this lithology. These pink granitoids dominate the population across the southern Hudson Mountains (Groups I and II of Johnson et al.²⁴; see their Fig. 10). Maish Nunatak is the only site north of Larter Glacier (Fig. 3a) where any pink granitoid erratics were observed²⁴, and they appear to form the entire population at that site²⁴. Erratics of tonalite lithology (typically pale grey in colour) are confined to sites north of Larter Glacier. Koehler Nunatak (Fig. 3a) was not visited by the authors, but field notes held by the Byrd Polar Rock repository ²⁵ associated with sample IGSN:PRR050701 state that granitic erratics, of unknown detailed petrology, are also abundant there.

Uniquely at World's End Bluff in the southern Hudson Mountains (Fig. 3a), we observed pink granite clasts within the basaltic bedrock (Fig. 2b). The relatively angular margin of the clasts, in contrast to the perched erratics which are generally rounded²⁴, implies that during the eruption that deposited the tuff, fragments of the local basement (granite) were ripped from the vent walls. An alternative explanation for the presence of granite clasts within the bedrock is that they were derived from underlying till. However, in the latter situation, the clasts would be expected to be

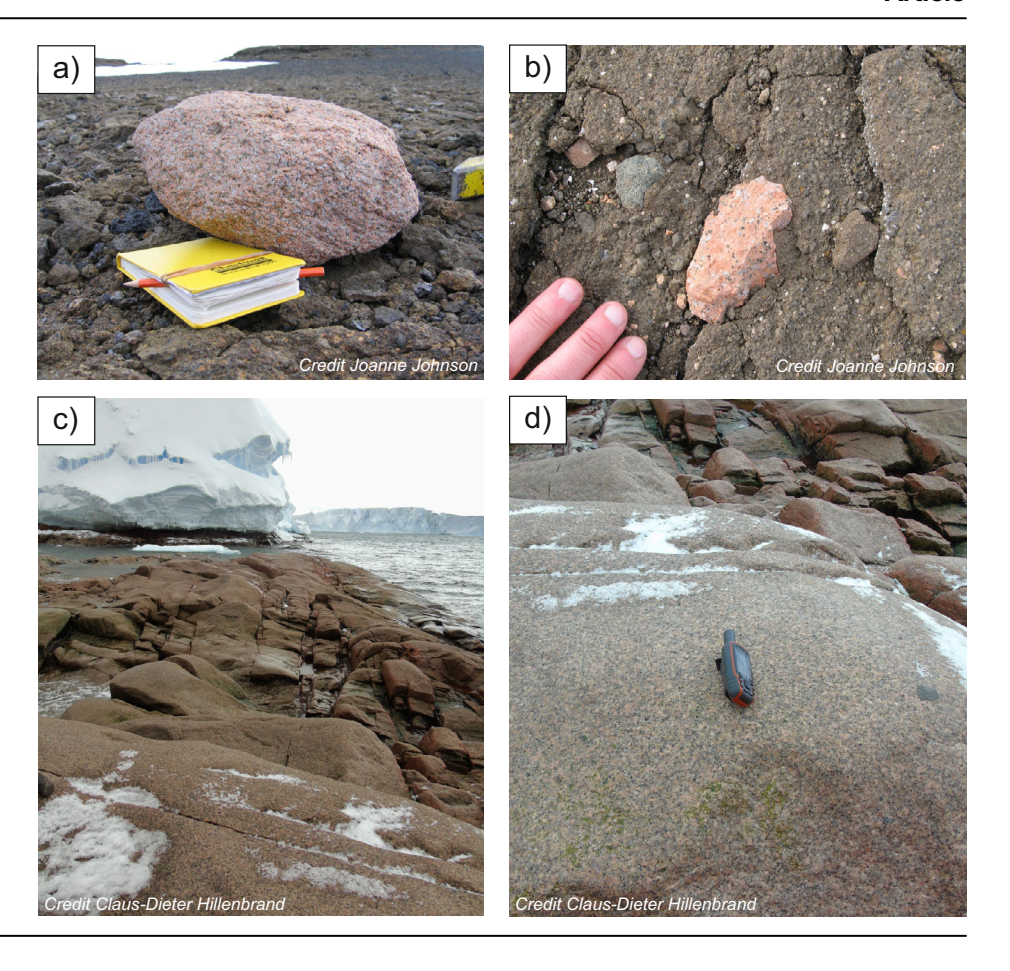
more rounded due to erosion during their earlier glacial transport (cf. erratics). Regardless of their precise origin, the presence of pink granite clasts within the volcanic bedrock at this site indicates that this lithology must have been present locally at the time of eruption, most likely as deeper bedrock beneath the volcanic layer. Pink granite with the same petrographic characteristics also crops out as bedrock at Sif Island²⁶ (Fig. 2c, d) on the southern side of PIG (Fig. 1b) and on islands in Pine Island Bay^{20,25}. Regionally, granite with similar properties also forms exposures adjacent to the Amundsen Sea Embayment in Marie Byrd Land^{20,27}, as well as in the Ellsworth-Whitmore Mountains²⁸ (Fig. 1a).

U-Pb zircon geochronology

U-Pb (zircon) geochronology was carried out on 10 of the selected 12 glacial erratic granitoids to determine their crystallisation age (Supplementary Figs. S3–S12 and Table 1). Samples were distributed across the Hudson Mountains, with age data supporting analysis of their provenance.

Four distinct age populations were identified; the youngest population is mid-Cretaceous with two samples from Slusher Nunatak, north of Larter Glacier (Fig. 3a), recording ages of 109 ± 1 Ma (SLU-107) and 103.9 ± 1.1 Ma (SLU-109). Both mid-Cretaceous erratic cobbles are characterised by a minor population of mid-Cretaceous zircon antecrysts from magmatism in the interval 125-115 Ma; a common feature of mid-Cretaceous granitoids in West Antarctica²⁹. The dominant group is a Middle Jurassic age population evident from five erratic samples from across the Hudson Mountains. Samples from south of Larter Glacier at Meyers Nunatak (MEY-102), Mount Manthe (MM-02), Shepherd Dome (SHD-109) and Inman Nunatak (INM-102), and a sample from Siren Rock (SIR-103), north of Larter Glacier, all record ages in the range 179-171 Ma (Fig. 3a). Sample INM-102 has a more complex U-Pb history, characterised by metamict zircon with very high U (typically >3000 ppm), coupled with Pb loss and incorporation of common Pb (Supplementary Fig. S12). Two analyses plot on concordia and yield an age of 171.4 ± 4.4 Ma, which we interpret as the likely crystallisation age, and is consistent with other erratic samples from adjacent nunataks. Two samples from Evans Knoll (EVK-104) and Siren Rock (SIR-103) yield ages in the range 204-200 Ma and represent a separate Late Triassic/Early Jurassic population of granitoid

Fig. 2 | Examples of pink granite in the Pine Island Glacier region. a Pink granitic erratic (MM-02) perched on bedrock in the Hudson Mountains. Diameter of erratic is 35 cm. b Granitic clast within tuffaceous bedrock at World's End Bluff, note angular clast margin. c Pink granitic bedrock at Sif Island. Jointing is visible in the foreground. d Close-up view of Sif Island bedrock (handheld GPS for scale); this is the same bedrock surface that is visible in the lower right corner of (c).



cobbles. A fourth age population is defined by only one sample from close to Winkie Nunatak (UNN-106), which yields a mid-Triassic age of 229. $8\pm1.4\,\mathrm{Ma}$ (Supplementary Fig. S10).

The four age populations identified in the erratic suite of the Hudson Mountains are well represented in the exposed granitoids of West Antarctica (Fig. 3b). Triassic granites have been identified from the Jones Mountains (c. 215-208 Ma³⁰) and Thurston Island (c. 239 Ma³¹) to the north of the Hudson Mountains (Fig. 1a). Also, a Late Triassic age (c. 208 Ma) has been reported for a micaceous granite from the southern Ellsworth-Whitmore Mountains²⁸ (Fig. 1a). Middle Jurassic magmatism has been recognised from Thurston Island³¹ and extensively across the Ellsworth-Whitmore Mountains^{28,32} (Fig. 1a). The ages in the Ellsworth-Whitmore Mountains have been determined from a broad selection of weakly foliated pink-grey granites and yield ages in the range 177-174 Ma, based on U-Pb (ID-TIMS)28, while U-Pb (SIMS) dating gives an age of $178.0 \pm 3.5 \,\mathrm{Ma^{32}}$. Granite from the more local Sif Island (Figs. 1b and 2c) also yields Middle Jurassic ages in the range 177-174 Ma²⁶. However, the Sif Island granite has been interpreted to have a closer affinity to granitoids of Thurston Island and the Antarctic Peninsula than the Ellsworth Mountains, based on Sr-Nd-Hf data²⁶. Mid-Cretaceous magmatism is widespread across West Antarctica, with granitoids reported from across Marie Byrd Land, particularly in the intervals 118-100 Ma³³⁻³⁵. Mid-Cretaceous granitoids are also reported from the central Amundsen Sea Embayment³⁶, Thurston Island³¹ and the southern Antarctic Peninsula²⁹, with a peak in granitoid magmatism recorded from 115 to 105 Ma.

Apatite fission track and (U-Th-Sm)/He ages

To complement the provenance analysis provided by U-Pb geochronology, we also determined apatite fission track (AFT) and (U-Th-Sm)/He (AHe) ages for a subset of the samples, providing information about their thermochronology (uplift and cooling history) (Table 1). We selected samples that are representative of the mid-Cretaceous, Middle Jurassic and Triassic

erratic groups. AFT data provide information on the low-temperature cooling history of the granitoids yielding valuable information on the most recent uplift and burial histories of their source region. Resulting thermal histories provide another check on the likely provenance of the Hudson Mountains erratics, particularly for potential source regions that have similar granitoid ages but have undergone differing exhumation histories. The AFT data are consistent across all granitoid populations with central ages in the range 130-90 Ma (Table 1, Supplementary Table S2 and Supplementary Fig. S13). Relatively long fission track lengths of 13-14 µm indicate rapid cooling and uplift to shallow crustal levels between 130 and 90 Ma. AHe analyses yielded mean Cretaceous cooling ages in the range 73-95 Ma. These slightly younger ages are consistent with the AFT results, which reflect a slightly higher (deeper) closure temperature. Bayesian Markov Chain Monte Carlo inversions³⁷ of samples with a suitable number of fission track length measurements and AHe data confirm high probability thermal histories consistent with rapid post-magmatic cooling to shallow crustal levels (Supplementary Fig. S14).

Thermochronometric data have also been reported from several sites across West Antarctica including Marie Byrd Land, Thurston Island, and the central Amundsen Sea Embayment^{26,38–40} (Fig. 3b). These data provide valuable additional constraints alongside our data from the Hudson Mountains erratic cobbles. All investigations highlight a rapid cooling event during the Early to mid-Cretaceous with very little uplift or burial occurring after this. Many authors have recognised the ubiquity of the mid-Cretaceous (100–90 Ma) cooling event along the length of the proto-Pacific margin of West Antarctica. For example, bedrock thermochronological dates from the Pine Island Bay area^{26,40} are remarkably similar to our results from the erratic cobbles and yield correspondingly comparable thermal history inversions.

Geophysical maps and modelling

Magnetic and gravity data reveal information about the rocks hidden beneath the ice. Magnetic anomalies reflect a combination of magnetic

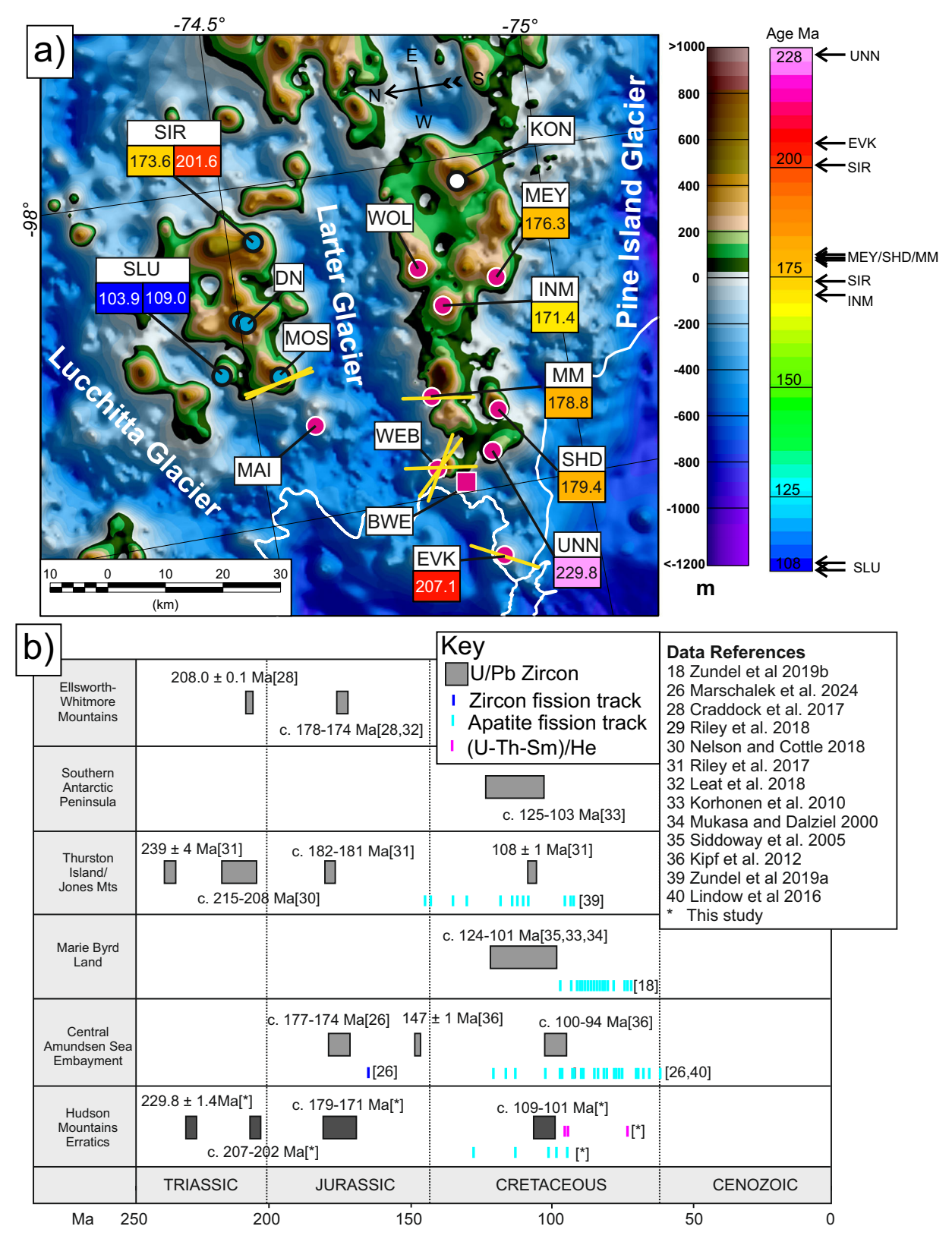


Fig. 3 | Age and lithology of intrusive rocks in West Antarctica. a Map of Hudson Mountains showing subglacial topography with erratic lithology (pink = pink granite, blue = pink granite absent, white = granites but with no petrological detail) and U-Pb ages (numbers in boxes—fill colour proportional to age). Arrows on age colour bar indicating clustering of U-Pb ages. Pink square locates pink granitic clasts within basaltic tuff (see Fig. 2b). White line marks coast/edge of ice shelf. SIR Siren Rock, SLU Slusher Nunatak, DN Dean Nunataks, MOS Mount Moses, MAI Maish

Nunatak, WOL Wold Nunatak, MEY Meyers Nunatak, INM Inman Nunatak, MM Mount Manthe, SHD Shepherd Dome, UNN Winkie Nunatak, EVK Evans Knoll, BWE World's End Bluff, WEB Webber Nunatak, KON Koehler Nunatak. **b** Ages from intrusive rocks cropping out across West Antarctica. Light grey bars mark U-Pb ages from the literature. Dark grey shading represents U-Pb ages from this study. Dark and light blue bars mark zircon fission track and apatite fission track ages, respectively. Pink bars indicate (U-Th-Sm)/He ages.

Table 1 | Summary of U-Pb, apatite fission track and (U-Th-Sm)/He analytical ages

Sample ID	U-Pb age (Ma) ± 1σ	Central AFT age (Ma) ± 1σ	Mean track length (μm)	Mean AHe age (Ma) ± 1σ
EVK-104	207.1 ± 1.4	n.a.	n.a.	n.a.
UNN-106	229.8 ± 1.4	n.a.	n.a.	n.a.
SHD-109	179.4 ± 1.5	113 ± 11	13.0 ± 0.2	n.a.
INM-102	171.4 ± 4.4	n.a.	n.a.	n.a.
MEY-102	176.3 ± 1.7	128 ± 11	13.8 ± 0.3	94.5 ± 15.1
MM-01	178.8 ± 2.3	n.a.	n.a.	n.a.
SIR-103	201.6 ± 1.1	101 ± 5	13.11 ± 0.11	95.4 ± 3.6
SIR-109	173.6 ± 1.6	98 ± 12	n.d.	n.a.
SLU-107	109 ± 1	n.a.	n.a.	n.a.
SLU-109	103.9 ± 1.1	94 ± 5	13.79 ± 0.08	73.1 ± 6.0

n.a. Not analysed, n.d. no data

susceptibility (how much a rock becomes magnetised by the Earth's field) and magnetic remanence (permanent magnetisation 'frozen' into magnetic minerals such as magnetite). Gravity anomalies, after correction for the signature of topography and crustal thickness, reflect the relative density of the rocks in the crust. Subglacial physiography, geological boundaries, and lithologies can therefore be interpreted from maps of airborne magnetic and gravity data, in conjunction with modelling and geological information (see 'Methods' and Fig. 4a, b). The mapped Airy isostatic gravity anomaly (Fig. 4a) shows a broad negative of ~20 mGal extending from the PIG Highlands, across PIG and into the southern edge of the Hudson Mountains. The negative structure appears continuous close to the grounding line, while further inland the anomaly is split by a low amplitude gravity high. In the central and northern Hudson Mountains, a large positive gravity anomaly of ~30 mGal is seen (Fig. 4a, e). Magnetic data show positive anomalies with amplitudes of 200-400 nT and widths of 25-50 km south of the PIG Highlands (Fig. 4b, d). These were previously interpreted as Cretaceous mafic intrusive rocks², and a similar magnetic anomaly is apparent beneath the inboard part of PIG. In contrast, magnetic anomalies near exposed mafic volcanic rocks in the Hudson Mountains are very high amplitude (>1500 nT), but narrower (<10 km) (Fig. 4d). Thus, our data suggest a different interpretation is required in the Hudson Mountains, relative to the interpreted Cretaceous mafic intrusive rocks to the south.

We investigated the sub-surface geology in more detail by constructing a 2D forward model of the gravity and magnetic fields observed along a survey flight line to maximise data resolution (Fig. 4d-f). This model was informed by field observations of rock outcrops and the presence and lithology of the observed erratics. The 2D forward model indicates that the observed high frequency magnetic anomalies in the Hudson Mountains can be created by a magnetic layer one to two kilometres thick. Susceptibility is modelled to vary latterly, from 0.009 to 0.026 SI (Table 2), broadly in-line with the measured mean and maximum susceptibility of 0.00127 and 0.0124 SI, respectively 25. The highest susceptibility is required north of Larter Glacier (Fig. 4c), directly above a modelled dense and magnetic body between 3 and 6 km depth (Fig. 4f, and Table 2). The highest susceptibility values in the model exceed measurements and may indicate a component of remnant magnetisation, i.e., permanent magnetisation retained by specific minerals. As our model does not consider magnetic remanence, a higher effective susceptibility is used to match the data.

The Hudson Mountains, south of Larter Glacier, are modelled to be underlain by a low-density body up to ~8 km thick. Within the mountains, this body is modelled to be overlain by volcanic rocks, as exposed at Wold Nunatak, but towards PIG the low-density body is modelled at the ice-bed interface. Our profile model suggests this low-density body is separated from a similar body south of PIG by a block of higher density and

susceptibility. However, the gravity anomaly map suggests these low-density bodies are joined out of the plane of the model (Fig. 4a). At the southern end of the modelled profile, a higher density and susceptibility body is required to match the observed data, consistent with previous interpretation of the geology in the Thwaites Glacier region².

Discussion

Linking field observations to our geochronology and thermochronology data and geophysical modelling enables us to provide fresh insights into the subglacial geology and past ice flow in the PIG region.

Based on variations in erratic lithologies and age between the northern and southern Hudson Mountains, at least two distinct source provinces are identified, broadly separated across Larter Glacier. The southern Hudson Mountains erratic province is dominated by U-Pb (crystallisation) ages of ~175 and ~205 Ma, and abundant pink granite. Field evidence that pink granite basement exists close to the Hudson Mountains (from the clasts entrained in volcanic deposits at World's End Bluff and outcrops at Sif Island) would be consistent with a relatively local source for the southern erratic province. The relatively large size of many of the observed erratics (>50 cm diameter in several cases, and >100 cm diameter in a few ²⁴) is also consistent with transport from a relatively local source, as fracturing during transport reduces clast size⁴¹. Although the reported age population and petrology (Fig. 2b) matches that of granitoids from both the Ellsworth-Whitmore Mountains and Thurston Island, neither of those locations is a plausible source. Ice transport from the Ellsworth-Whitmore Mountains is not viable as those outcrops are 500 to 600 km away from the Hudson Mountains. Furthermore, flow to the erratic sites would have had to cross the PIG trough, which models indicate remained a major glacial outflow at the LGM42,43 diverting any material transported from the Ellsworth-Whitmore Mountains towards the ocean. Thurston Island is an unlikely source for the observed pink granite erratics, as it would require ice flow inland from the known coastal outcrops at the LGM.

The U-Pb ages of erratics deposited on nunataks adjacent to Lucchitta Glacier are the youngest in the mountain range (109–101 Ma) and are confined to the northern Hudson Mountains erratic group, which lacks pink granites. Such ages are most like rocks cropping out in the southern Antarctic Peninsula and central Amundsen Sea Embayment (Fig. 3b). This finding implies that the erratics of the northern province were also derived from a relatively local (presently subglacial) source. However, the difference in age and lithology points to a source distinct from the erratics in the southern Hudson Mountains. This is in-line with the flow pathways of both the modern and LGM ice sheets which show distinct source regions for erratics in the two areas (Supplementary Fig. S15). The interpretation of a local source for both the northern and southern Hudson Mountains erratics is supported by the comparable thermochronometry data between erratics and from the wider Amundsen Sea region 26,38,44, which exhibit a very similar uplift and cooling history.

We use the observations of abundant, most likely locally sourced, pink granitic glacial erratics in the southern Hudson Mountains to define the age and lithology of the low-density body identified in the geophysical models beneath the southern Hudson Mountains. The sampled erratics (Fig. 3a) show a strong clustering in U-Pb ages at $\sim\!175\,\mathrm{Ma}$. Thermochronological results indicate that both the northern and southern erratics cooled rapidly in the mid-late Cretaceous, then unroofed slowly until the present day (Supplementary Fig. S14). These data and thermal history inversions support previous interpretations that cooling in this area was likely facilitated by a pulse of tectonic denudation, potentially along the PIG rift, followed by relative quiescence from the Palaeocene until at least the Miocene 40,44 .

At present, the Hudson Mountains pink granitic body must outcrop at the ice bed interface for the erratics to have been eroded from it. However, the presence of granite xenoliths/rip-up clasts within tuffaceous bedrock cropping out at World's End Bluff (Figs. 2b and 3a) is also consistent with our geophysical model for a volcanic layer that locally overlies the granite. Our gravity anomaly map (Fig. 4a) suggests that the interpreted granite extends southward across PIG, supporting the previous interpretation of the

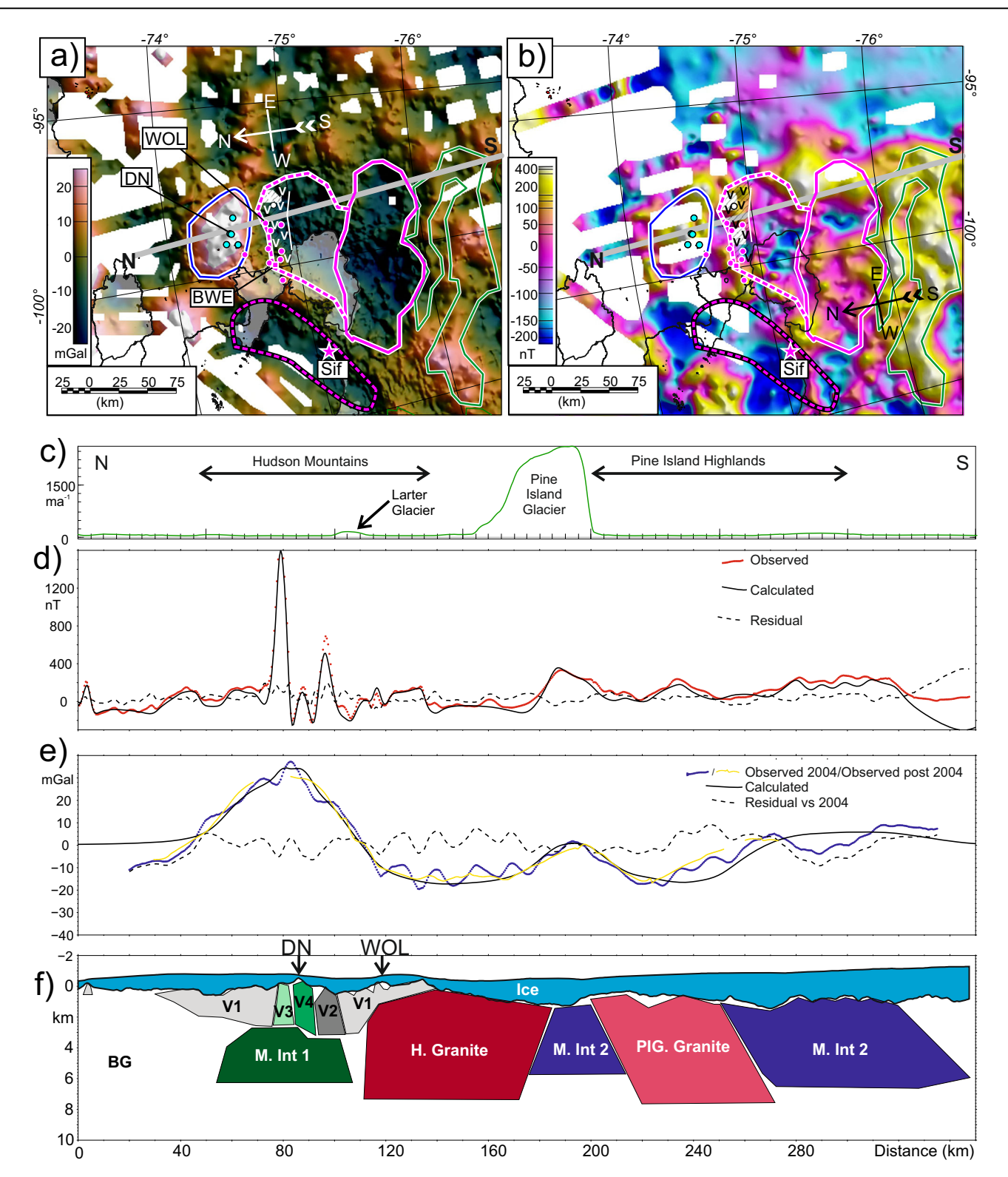


Fig. 4 | **Geophysical data, modelling and interpretation. a** Airy isostatic gravity anomaly from data compilation. Grey line shows modelled flight line. Pale shading marks ice shelves where the gravity corrections for topography/bathymetry are considered less robust. Approximate interpreted geological boundaries include: Previously interpreted Cretaceous mafic intrusive body (solid green line) and un-dated subglacial granite (solid pink line)². From this study a 3–8 Ma mafic body (blue), southern edge of 3–8 Ma subglacial volcanics (V pattern and white line), northward extension of ~175 Ma granite (pink/white dashed line), and extent of Sif Island granite (pink/black dashed line). **b** Total field magnetic anomaly continued to an altitude of 2500 m. Boundaries same as (a). **c** Ice velocity along modelled N to S profile located in (a, b).

d Profile magnetic anomalies. Observed data continued to an altitude of 2000 m and modelled assuming the same observation altitude. e Airy isostatic gravity anomaly. Blue line is profile data from 2004 continued to 2000 m. Yellow line is the gravity anomaly sampled from the compilation created for this study, dominated by more recent data. Black line shows modelled gravity anomaly at 2000 m observation altitude. f Joint upper crustal model. Note coloured bodies have density and susceptibility distinct from background values. Grey bodies only have susceptibility variations. Interpreted lithologies include: volcanics (V1-4), mafic Intrusive rocks (M. Int 1 and 2), and granites (H. Hudson Mountains, PIG Pine Island Glacier). BG indicates background. Modelled density and susceptibility values in Table 2.

Table 2 | Magnetic susceptibility and density of modelled upper crustal lithologies shown in Fig. 4f

Name	Abbreviation in Fig. 4	Magnetic susceptibility (SI)	Density kgm ⁻³
Background/Ice	BG/Ice	0.0000	2670
Volcanic	V1	0.0090	2670
Volcanic	V2	0.0160	2670
Volcanic	V3	0.0260	2800
Volcanic	V4	0.0110	2800
Hudson Mafic intrusion	M. Int 1	0.0015	2900
Hudson Granite	H. Granite	0.0040	2600
PIG Granite	PIG. Granite	0.0070	2600
Mafic intrusion 2	M. Int 2	0.0090	2700

highlands south of PIG as granitic². The dominant ~175 Ma age for the observed erratics suggests this is the most likely crystallisation age for the wider granite body spanning PIG. In addition, we interpret the gravity low around Sif Island (Fig. 4a) as a distinct, but broadly contemporaneous, episode of granitic plutonism. Together, the dating and geophysical evidence presented here expands the region of West Antarctica impacted by the ~175 Ma magmatic event, attributed to a major thermal anomaly associated with the breakup of Gondwana⁴⁵. In addition, the continuation of the ~175 Ma granite body across PIG implies limited motion along the proposed Cretaceous or younger PIG rift⁴⁶. Although the pink granitic erratics are dominated by crystallisation ages of ~175 Ma, samples with ages of ~205 Ma and ~223 Ma are also present, indicating that alkaline granitic magmatism with this geochemistry had been active in this region for almost 50 Myrs, a similar pattern to that observed in the Ellsworth-Whitmore Mountains²⁸.

Evidence that ice flowed over the Hudson Mountains comes from both the perched erratics and striations observed on exposed bedrock surfaces. At five out of the seven sites where striated bedrock was recorded, the striations are oriented broadly N-S (Fig. 5) indicating that thick (erosive) ice flowing approximately N-S must have covered the area in the past. This was probably during the LGM (~20 ka) when the ice sheet was substantially thicker than today^{22,47}. The distribution of the abundant pink granitic erratics supports northward ice flow, as this flow direction would carry material plucked from the modelled subglacial granite - indicated by the distinct negative Airy isostatic gravity anomaly (Fig. 4a, f) - into the southern Hudson Mountains. Such dominantly northward flow agrees with the best fitting modelled palaeo ice sheet surface slope (and hence presumed flow direction) at 20 ka from the Parallel Ice Sheet Model (PISM)⁴³ (Fig. 5a). Flow pathways based on the modelled LGM ice surface slope show clear paths from the flank of PIG, where the granite is modelled to be at the ice bed interface, into the mountains where the erratics were deposited (Supplementary Fig. S15a, b). In contrast, at the present day, ice flow is mostly channelled E-W along troughs occupied by Pine Island and Larter glaciers, and NE-SW along the Lucchitta Glacier (Fig. 5b), with flow paths restricted to within the southern Hudson Mountains (Supplementary Fig. S15c, d). The change from palaeo to approximately modern flow direction must have occurred by 7-8 ka^{21,22}, when the glacial erratics were exposed.

The modelled palaeo flow at 20 ka in the best fitting PISM model⁴³ is generally aligned with the observed bedrock striations and is consistent with northward transport of pink granite erratics. However, we note that neither the N-S oriented striations at Mount Moses nor the presence of abundant pink granite erratics derived from the south at the adjacent Maish Nunatak are consistent with the simulated LGM flow directions⁴³ (Fig. 5a and Supplementary Fig. S15a). A more detailed high-resolution model of the LGM ice sheet constrained by the flow pattern suggested by our field observations, geochronology and geophysics, would thus provide a better representation of past ice sheet evolution, and hence have the potential to improve

predictions of future change. At Evans Knoll, where striations are (in contrast to other areas) closely aligned with the present ice flow direction (Fig. 5b), the exposure history of the striated bedrock surfaces is not known (no exposure dating has yet been undertaken on bedrock in the Hudson Mountains). Thus, we cannot be certain when these striations were formed. However, their orientation approximately parallel to present-day ice flow and orthogonal to LGM ice flow (Fig. 5a) suggests they may originate from a later stage of erosion when ice flow was closer to its present configuration.

The primary conclusions of our study are that a ~175 Ma granite body extends across PIG and that ice flowed across the southern Hudson Mountains in a different orientation at the LGM from today, depositing erratics derived from local subglacial bedrock rather than from a bedrock source far upstream. In addition, we conclude that combining multiple geological approaches that target the subglacial environment can enhance our understanding more than would be achieved by using them in isolation. We have demonstrated that a joined-up approach combining field observations, geological dating methods and geophysical modelling can provide valuable information needed to constrain and validate ice sheet models, improving their ability to reliably project future sea level contributions from the Antarctic Ice Sheet⁴⁸. Considering the pace of ongoing ice sheet retreat in the Amundsen Sea sector⁴⁹ and its dominant contribution to global sea level rise from Antarctica both now and expected in coming centuries⁵, such refinements are especially critical for this region. Specifically, the understanding that the down-stream base of PIG is likely granitic—rather than a thick (>100 s of m) sedimentary basin— changes how erodibility, basal deformation, ground water and ice interface hydrology are considered and parameterised in ice sheet models of the area. In addition, by revealing palaeo flow directions, we help constrain which are the most realistic models of past ice flow in the area, and hence which models and parameterisations will likely provide the most reliable estimates of future change.

Since glacial erratics are extremely common in Antarctica (Supplementary Fig. S1), there is great potential to conduct similar studies elsewhere. Even though deep subglacial access drilling will provide increasing opportunities to recover geological samples from beneath ice sheets in the coming years, since erratics occur above the ice surface, they are more easily accessible in the field and therefore provide a viable alternative method for improving knowledge of subglacial geology. More than 100 closely-spaced erratics have been collected from each of the Transantarctic Mountains, the Ellsworth and Pensacola mountains in the Weddell Sea Embayment, Mount Murphy in the central Amundsen Sea Embayment, and the Grove Mountains adjacent to Amery Ice Shelf (Supplementary Fig. S1). These sites are therefore ripe for further investigation. In contrast, very few glacial erratics from the region between George V Land and Wilkes Land (Supplementary Fig. S1) have been sampled; this remote region is very difficult to access, making their occurrence and distribution difficult to assess. Expected advances in machine learning methods will in future afford opportunities to reliably identify the presence of erratics and map their distribution⁵⁰. Airborne⁵¹ or satellite^{52,53} remote sensing methods may in addition allow the lithologies of erratics to be determined without needing to undertake fieldwork, and if higher resolution imagery is available in future, may also be easier able to resolve individual erratics. Together, these approaches will add to the inventory of information from erratics that can be used to increase knowledge of the subglacial environment and will enable better targeting of future sampling campaigns.

Methods

Field sampling of glacial erratics and observations of geological

Cobbles and boulders entrained within ice (known as glacial erratics) are commonly collected for cosmogenic nuclide surface exposure dating to determine ice sheet thinning history. Several field campaigns in the Amundsen Sea sector of Antarctica have been undertaken with this purpose since 2006. In total, 90 erratics have now been sampled from the Hudson Mountains²⁴. The majority have yielded mid-Holocene ¹⁰Be exposure ages, implying that the Hudson Mountains were deglaciated within the past

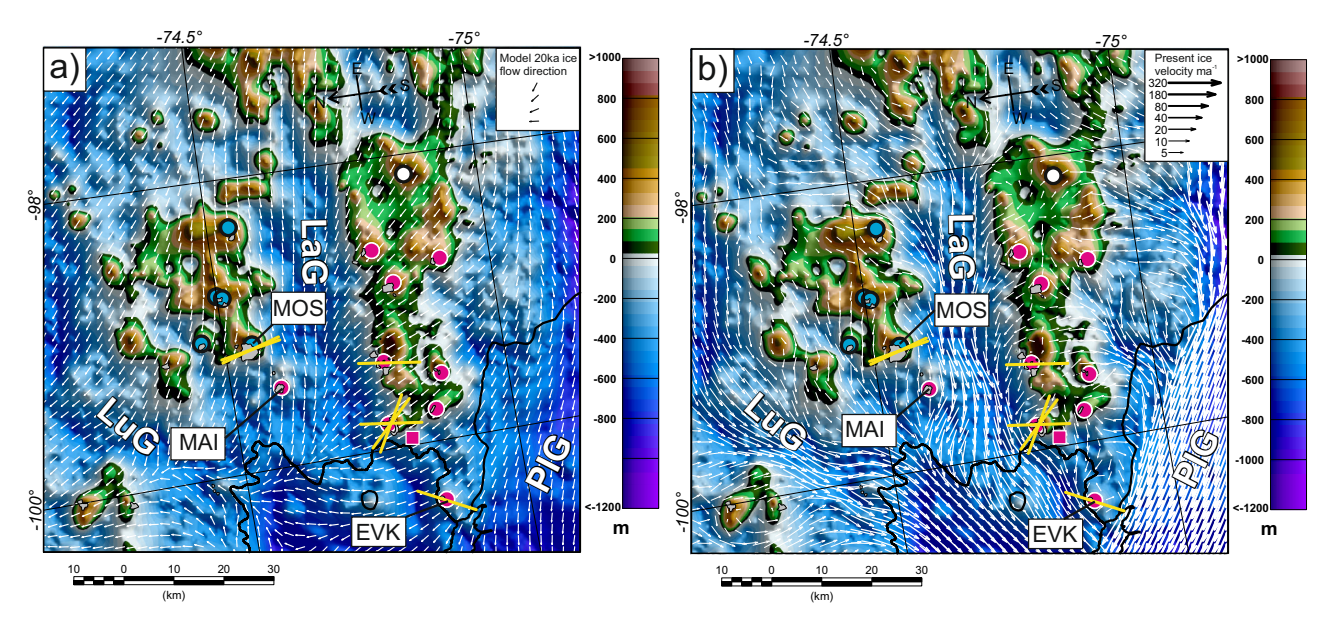


Fig. 5 | Past and present ice flow directions across the Hudson Mountains. a Ice flow directions at 20 ka derived from modelled ice surface slope⁴³, overlain on bed elevation. b Present day ice flow direction⁷⁴ overlain on bed elevation. White labels

indicate nunataks: Mount Moses (MOS), Maish Nunatak (MAI), Evans Knoll (EVK). Lucchitta Glacier (LuG), Larter Glacier (LaG). Yellow lines show striation orientations²⁴.

10 ka^{20–22}. These cobbles and boulders show abundant evidence of glacial transport (rounding, faceting and striations) and are perched on scoured bedrock surfaces or regolith, rather than embedded in lodgement till²⁴.

For this study, we chose a subset of 12 erratics (Supplementary Table S1 and Supplementary Fig. S2) that are representative of all three groups previously detailed that is, erratics collected from adjacent to each outlet glacier in the area (Pine Island, Larter and Lucchitta glaciers; Fig. 1)—and representing the range of lithologies present (syenite, alkali granite, granite, granodiorite, tonalite; determined using a visual estimation of the modal proportions of constituent minerals plotted on a Quartz, Alkali feldspar, Plagioclase and Feldspathoid (QAPF) diagram⁵⁴; see Supplementary Table S1 and previous paper²⁴ for details). Although a few gabbroic erratics are also present, gabbro is not suitable for U-Pb dating due to the absence of zircon, thus, we did not include any of those erratics in our study. Of the 12 samples selected, only 10 were found to contain zircons making them suitable for dating (see below for separation and dating methods).

Detailed field observations of the geological and geomorphological setting of the erratics (e.g. outcropping bedrock lithology and similarities/ differences between nunataks, presence of striated bedrock surfaces and orientation of striations, elevations and lithologies of erratics, and evidence for glacial transport) were collected prior to sampling for exposure dating. Such observations are important for understanding the broader glacial-geological context of the region, and in particular for determining what inferences can reasonably be made about the subglacial geology and environment from the erratics. We used these observations to help interpret the origin of the erratics we analysed for geochronology and thermochronology.

U-Pb zircon geochronology

We used zircon U-Pb geochronology to determine the crystallisation age of the granitoid erratic cobbles from the Hudson Mountains. A subset (10 samples; those containing zircon—see above) of the glacial erratic cobbles were dated. Zircon was separated from the samples by passing the <250 µm fraction through standard density liquids and Frantz magnetic separation procedures to concentrate the zircon fraction, which was then mounted in hard epoxy resin before being polished for analysis by laser ablation inductively coupled mass spectrometry (LA-ICP-MS) (Agilent 7900 coupled to a New Wave Research 193 nm excimer laser) at the London Geochronology Centre based in University College London, UK. Typical

laser spot sizes of 25 µm were used with a 7-10 Hz repetition rate and a fluence of 2.5 J/cm². Background measurement before ablation lasted 15 s and laser ablation dwell time was 25 s. The external zircon standard was Plešovice, which was used to correct for instrumental mass bias and depthdependent inter-element fractionation and has a Thermal Ionization Mass Spectrometry (TIMS) reference age 337.13 ± 0.37 Ma⁵⁵. The secondary standard was GJ1, used to verify the accuracy of the data, which has a TIMS reference age 601.86 ± 0.37 Ma⁵⁶. Standard errors on isotope ratios and ages include the standard deviation of ²⁰⁶Pb/²³⁸U ages of the Plešovice standard zircon. Time-resolved signals that record isotopic ratios with depth in each crystal were processed using GLITTER 4.5, data reduction software, developed by the ARC National Key Centre for Geochemical Evolution and Metallogeny of Continents (GEMOC) at Macquarie University and CSIRO Exploration and Mining. We calculated ages using the ²⁰⁶Pb/²³⁸U ratios for samples dated as <1.1 Ga. Discordance was determined using (207 Pb/235 U -²⁰⁶Pb/²³⁸U) / ²⁰⁶Pb/²³⁸U) and similar for ²⁰⁷Pb/²⁰⁶Pb ages. The results are presented in Table 1, Supplementary Figs. S3-S12 and associated data repository at the UK Polar Data Centre⁵⁷.

Apatite fission track and (U-Th-Sm)/He thermochronology

To determine rock cooling histories, we analysed four samples with suitable apatites for fission track (AFT) age (full results reported in Supplementary Table S2) and a further three samples for (U-Th-Sm)/He (AHe) age. Thermochronometry analyses were carried out at the London Geochronology Centre, UK. Apatite grains were mounted in epoxy resin on glass slides and polished to expose grain internal surfaces. Samples were then etched in 5 N HNO $_3$ for 20 s at 20 ± 1 °C to reveal spontaneous fission tracks and counted using a Zeiss Axioplan optical microscope with a total magnification of ×1250. Grain uranium concentrations were analysed by LA-ICPMS with a session-specific zeta fractionation factor based on Durango apatite (reference age 31.44 ± 0.18 Ma (2 s) 59). Grain chlorine contents were also measured. Data were processed using IsoplotR 61 .

Each apatite (U-Th-Sm)/He analysis included at least five single-grain replicates. To reduce uncertainty associated with alpha ejection correction whole, inclusion- and fracture-free apatite grains were preferentially selected. Erroneous single grain dates (>2 σ from mean age) descend from poorer quality grains (e.g., broken or showing other defects) and are omitted from reported mean age calculations, which also include FT (alpha-ejection correction). Durango apatite was included in each sample batch. Samples

were placed in platinum tubes and outgassed using a 25 W, 808 nm diode laser and ^4He measured on a Hiden DLS-1 quadrupole mass spectrometer. Gas volumes were determined by isotope dilution using two 5800 cc vacuum tanks with pipette volumes of 0.3222 cc for the ^4He Standard and 0.2258 cc for ^3He . Following extraction, Pt tubes were placed in vials for apatite dissolution using a 50 μ l spike with a known concentration of ^{235}U , ^{230}Th and ^{149}Sm , which included HNO $_3$. Sample concentrations were measured on an Agilent 7900× ICP-MS. Spike solutions were re-calibrated for each session.

The QTQt software³⁷ based on a Bayesian trans-dimensional approach to data inversion was used to extract probable thermal histories. Input data included single-grain data and chemical characteristics. Model outputs are accepted thermal history models that can be combined to give an expected thermal history model, which is the mean of the accepted paths weighted by the posterior probability of each individual thermal history. This posterior distribution can also be used to define the 95% credible intervals that provide a measure of uncertainty. Model runs allowed the temperature offset to vary over time and data were predicted using the annealing and diffusion models^{62,63}.

Geophysical data compilation and modelling

The remote location of PIG and the Hudson Mountains means that, despite its importance, this region has been relatively poorly sampled by geophysical methods compared to elsewhere in Antarctica. To construct the most reliable geophysical maps showing the subglacial geology of the region, we combined airborne survey data from several field campaigns. Gravity data used in this study were collected by Operation Ice Bridge (OIB)⁶⁴ and the 2004/2005 joint UK/US surveys known as BBAS (UK)^{46,65} and AGASEA (US Airborne Geophysical Survey of the Amundsen Embayment)⁶⁶ (Supplementary Fig. S16). The OIB gravity dataset has an accuracy of ~1 mGal and was generally flown at a constant distance above the ice surface, while the older data were flown at set altitudes and have an accuracy of between 2.8 and 2.3 mGal. Free air gravity data were continued to a common altitude of 2000 m

We calculated the Bouguer correction for the gravity data using a prism based approach⁶⁷ at an observation altitude of 2000 m using a subset of the BEDMAP3 topographic compilation⁶⁸ extending at least 160 km from the margins of the study area. The Bouguer correction included a model for ice (915 kgm⁻³), water (1028 kgm⁻³), and rock above and below sea level (±2670 kgm⁻³). We subtracted this gravity model from the line free air anomalies to give the Bouguer anomaly. The Bouguer anomaly remains dominated by the signal related to isostatic compensation of the topography. To provide an approximation of the expected isostatic gravity field, we use an Airy isostatic model, assuming the crust has no lateral strength and that the associated gravity signal is from the Moho, which is at an average depth of 30 km. We subtracted this isostatic gravity field from the line Bouguer anomaly to give the Airy isostatic residual anomaly. A mean of 46 mGal was removed from the Airy isostatic residual to distribute the observed anomalies around zero within the study region. The final Airy anomaly was interpolated onto a 1 km mesh raster using a minimum curvature approach. Although there are many assumptions in our calculation of the Airy isostatic model, it provides a simple and repeatable estimate of the impact of isostatic compensation. Errors in our isostatic assumptions will only impact the long wavelength signal and should not distort the model of upper crustal features.

Magnetic data were taken from the line data released with ADMAP2 69 , and integrated in a previous compilation 2 . We interpolated these data onto a 1 km mesh raster for display. In addition, we upward continued line data to an elevation of 2000 m, to facilitate joint modelling with the gravity data.

To determine the subsurface geology using potential field data, we constructed a 2D forward model of the crustal structure using the open-source GMGPY software tool (https://github.com/btozer/gmg/). This allows modelling of arbitrary 2D bodies with fixed density and susceptibility contrast using line integral methods^{70,71}. As models of potential field data are non-unique, we did not aim to create a definitive, or statistically best fitting model. Instead, we aimed to test if a simple geometry with assumptions about subglacial lithology supported by observations can provide a

geologically plausible model. The final model had a RMS error of 4.4 mGal compared to the observed gravity data. The magnetic model had an RMS error of 84 nT, reflecting the extremely high amplitude magnetic anomalies, which could not be fit well by our simple model. The observational data were taken from a specific 2004 BBAS survey line (Supplementary Fig. S16). This single dataset includes magnetics, gravity and radar data extending ~360 km over the central Hudson Mountains, the adjacent PIG and other subglacial highlands. More recent gravity data from OIB indicates there may be ~20 km wavelength noise in the BBAS gravity signal, but the more recent and accurate data are not complete along the full survey line, limiting its utility for constraining a regional model.

To constrain the model, we made a series of assumptions. First, where possible, source bodies have both a density and susceptibility contrast to background. This reduces the degree of freedom within the model, as both gravity and magnetic data must be fit by the same bodies. Background density was assumed to be 2670 kgm⁻³, matching the Bouguer correction density, which is a reasonable global approximation for the density of the upper crust. Background susceptibility was set to zero. Values for magnetic susceptibility²⁵ and density⁷² from local exposed rocks held in Antarcticwide compilations were considered when defining the modelled sources, where possible. Where the erratics indicate a specific subglacial lithology with no local density measurement, such as the pink alkali granites, density values for rocks with this apparent lithology in the Ellsworth-Whitmore Mountains from the Petrochron database were used⁷². Modelled bodies were generally considered to extend from the surface to the depth required to match the observed data. This resulted in modelled sources extending from the ice-bed interface to a depth of 6-8 km. This maximum depth is, however, not definitive, since the density of the surrounding rock is not well constrained. For example, larger negative density contrasts, as assumed, for example, for the Cornubian granitic batholith⁷³, would lead to thinner modelled granitic bodies. In addition to the assumptions above, we aimed to minimise the complexity of the bodies. Complex sources and superposition of bodies is permissible by the data, but an overly complex model is not justified without further independent constraints such as seismic or magnetotelluric (MT) data. Using the assumptions laid out above constrains the 2D model to be as geologically realistic as it can be.

Construction of past and present ice flow paths

To constrain the possible source of the erratics that now lie in the Hudson Mountains, we 'backtrack' from their current location using the modelled and observed directions of ice flow (Fig. 5). For the present day scenario, we used the MEASURES 2017 ice velocity dataset⁷⁴. For palaeo ice flow, we assume ice flow follows the surface slope of the modelled ice sheet from a published best-fitting PISM model run⁴³. To create the ice flow paths, we iterated upstream from each erratic location along the presumed ice flow vector. We moved upstream in 2 km steps, assessing flow direction at each point. This method is robust where ice flow is fast. However, in the modern case where ice flow is slow or very complex, this method can move the flow line in random directions, where noise exceeds flow velocity, or allow the flow path to jump between catchments. We therefore edited the predicted modern flow lines so that they are consistent with the ice flow vector field (Supplementary Fig. S15).

Reporting summary

Further information on research design is available in the Nature Portfolio Reporting Summary linked to this article.

Data availability

Aerogeophysical data collected by the British Antarctic Survey forming the basis of this study are available from the UK Polar Data Centre (UKPDC) including; gravity⁶⁵, magnetic⁷⁵ and radar data⁷⁶. Other geophysical datasets are available from the sources cited in the text. New geochronological data associated with this study are also available from the UKPDC⁵⁷. Details of erratic lithology and striated bedrock surfaces in the Hudson Mountains are previously published^{77,78}.

Received: 23 April 2025; Accepted: 10 September 2025; Published online: 22 October 2025

References

- Bell, R. et al. Influence of subglacial geology on the onset of a West Antarctic ice stream from aerogeophysical observations. *Nature* 394, 58–62 (1998).
- Jordan, T. A., Thompson, S., Kulessa, B. & Ferraccioli, F. Geological sketch map and implications for ice flow of Thwaites Glacier, West Antarctica, from integrated aerogeophysical observations. Sci. Adv. 9. eadf2639 (2023).
- Smith, A. M., Jordan, T. A., Ferraccioli, F. & Bingham, R. G. Influence of subglacial conditions on ice stream dynamics: Seismic and potential field data from Pine Island Glacier, West Antarctica. *J. Geophys. Res.* 118, 1471–1482 (2013).
- Agrios, L. M. et al. Detrital geochronology and lithologic signatures of Weddell Sea Embayment ice streams, Antarctica – implications for subglacial geology and ice sheet history. GSA Bull. https://doi.org/10. 1130/B36117.1 (2021).
- Scambos, T. A. et al. How much, how fast? A science review and outlook for research on the instability of Antarctica's Thwaites Glacier in the 21st century. Glob. Planet. Change 153, 16–34 (2017).
- Balco, G. Technical note: a prototype transparent-middle-layer data management and analysis infrastructure for cosmogenic-nuclide exposure dating. Geochronology 2, 169–175 (2020).
- Stone, J. O. et al. Holocene deglaciation of Marie Byrd Land, West Antarctica. Science 299, 99–102 (2003).
- Simões Pereira, P. et al. The geochemical and mineralogical fingerprint of West Antarctica's weak underbelly: Pine Island and Thwaites glaciers. Chem. Geol. 550, 119649 (2020).
- Licht, K. J. & Hemming, S. R. Analysis of Antarctic glacigenic sediment provenance through geochemical and petrologic applications. *Quat.* Sci. Rev. 164, 1–24 (2017).
- Goodge, J. W., Fanning, C. M., Brecke, D. M., Licht, K. J. & Palmer, E. F. Continuation of the Laurentian Grenville Province across the Ross Sea Margin of East Antarctica. *J. Geol.* 118, 601–619 (2010).
- Licht, K. J., Hennessy, A. J. & Welke, B. M. The U-Pb detrital zircon signature of West Antarctic ice stream tills in the Ross embayment, with implications for Last Glacial Maximum ice flow reconstructions. *Antarct. Sci.* 26, 687–697 (2014).
- Licht, K. J., Lederer, J. R. & Jeffrey Swope, R. Provenance of LGM glacial till (sand fraction) across the Ross embayment, Antarctica. Quat. Sci. Rev. 24, 1499–1520 (2005).
- Palmer, E. F., Licht, K. J., Swope, R. J. & Hemming, S. R. in Mineralogical and Geochemical Approaches to Provenance (eds Rasbury, T., Hemming, S. & R. Riggs, N.) 0 (Geological Society of America, 2012).
- Diekmann, B. & Kuhn, G. Provenance and dispersal of glacial-marine surface sediments in the Weddell Sea and adjoining areas, Antarctica: ice-rafting versus current transport. *Mar. Geol.* 158, 209–231 (1999).
- 15. Pierce, E. et al. A comparison of detrital U–Pb zircon, 40Ar/39Ar hornblende, 40Ar/39Ar biotite ages in marine sediments off East Antarctica: implications for the geology of subglacial terrains and provenance studies. *Earth Sci. Rev.* **138**, 156–178 (2014).
- Roy, M., van de Flierdt, T., Hemming, S. R. & Goldstein, S. L. 40Ar/ 39Ar ages of hornblende grains and bulk Sm/Nd isotopes of circum-Antarctic glacio-marine sediments: implications for sediment provenance in the southern ocean. Chem. Geol. 244, 507–519 (2007).
- Simões Pereira, P. et al. Geochemical fingerprints of glacially eroded bedrock from West Antarctica: detrital thermochronology, radiogenic isotope systematics and trace element geochemistry in Late Holocene glacial-marine sediments. *Earth Sci. Rev.* 182, 204–232 (2018).
- Zundel, M. et al. A large-scale transcontinental river system crossed West Antarctica during the Eocene. Sci. Adv. 10, eadn6056 (2024).

- Fitzgerald, P. G. & Goodge, J. W. Exhumation and tectonic history of inaccessible subglacial interior East Antarctica from thermochronology on glacial erratics. *Nat. Commun.* 13, 6217 (2022).
- Johnson, J. S., Bentley, M. J. & Gohl, K. First exposure ages from the Amundsen Sea Embayment, West Antarctica: the Late Quaternary context for recent thinning of Pine Island, Smith, and Pope Glaciers. *Geology* 36, 223–226 (2008).
- 21. Johnson, J. S. et al. Rapid thinning of Pine Island Glacier in the early Holocene. *Science* **343**, 999–1001 (2014).
- Nichols, K. A. et al. Offshore-onshore record of Last Glacial Maximum-to-present grounding line retreat at Pine Island Glacier, Antarctica. *Geology* 51, 1033–1037 (2023).
- Rowley P. D., Laudon T. S., La Prade K. E. & W.E., L. in Volcanoes of the Antarctic Plate and Southern Oceans Vol. 48 (eds LeMasurier, W.E. & J. W. Thompson, J.W.) 289–293 (Antarctic Research Series, 1986).
- Johnson, J. S. et al. Glacial geology of the Hudson Mountains, Amundsen Sea sector, West Antarctica. Quat. Sci. Rev. 350, 109027 (2025).
- 25. The Polar Rock Repository (PRR) Byrd Polar and Climate Research Center (BPCRC), Ohio State University: Polar rock and dredge samples available for research and educational use from the PRR https://doi.org/10.7289/V5RF5S18 (2024).
- Marschalek, J. W. et al. Geological insights from the newly discovered granite of Sif Island between Thwaites and Pine Island glaciers. Antarct. Sci. 36, 51–74 (2024).
- Pankhurst, R. J., Weaver, S. D., Bradshaw, J. D., Storey, B. C. & Ireland, T. R. Geochronology and geochemistry of pre-Jurassic superterranes in Marie Byrd Land, Antarctica. *J. Geophys. Res.* 103, 2529–2547 (1998).
- Craddock, J. P. et al. Precise U-Pb zircon ages and geochemistry of Jurassic granites, Ellsworth-Whitmore terrane, central Antarctica. GSA Bull. 129, 118–136 (2017).
- Riley, T. R., Burton-Johnson, A., Flowerdew, M. J. & Whitehouse, M. J. Episodicity within a mid-Cretaceous magmatic flare-up in West Antarctica: U-Pb ages of the Lassiter Coast intrusive suite, Antarctic Peninsula, and correlations along the Gondwana margin. GSA Bull. 130, 1177–1196 (2018).
- Nelson, D. A. & Cottle, J. M. The secular development of accretionary orogens: linking the Gondwana magmatic arc record of West Antarctica, Australia and South America. *Gondwana Res.* 63, 15–33 (2018).
- Riley, T. R. et al. A revised geochronology of Thurston Island, West Antarctica, and correlations along the proto-Pacific margin of Gondwana. *Antarct. Sci.* 29, 47–60 (2017).
- Leat, P. T. et al. Jurassic high heat production granites associated with the Weddell Sea rift system, Antarctica. *Tectonophysics* https://doi. org/10.1016/j.tecto.2017.11.011 (2018).
- Korhonen, F. J., Saito, S., Brown, M., Siddoway, C. S. & Day, J. M. D. Multiple Generations of Granite in the Fosdick Mountains, Marie Byrd Land, West Antarctica: implications for polyphase intracrustal differentiation in a continental margin setting. *J. Petrol.* 51, 627–670 (2010).
- Mukasa, S. B. & Dalziel, I. W. D. Marie Byrd Land, West Antarctica: Evolution of Gondwana's Pacific margin constrained by zircon U-Pb geochronology and feldspar common-Pb isotopic compositions. Geol. Soc. Am. Bull. 112, 611–627 (2000).
- Siddoway, C. S., Sass, L. C. I. & Esser, R. in Terrane Processes at the Margin of Gondwana Vol. 246 Special Publication (eds Vaughan, A.P.M., Leat, P.T. & R. J. Pankhurst, R.J.) 417–438 (Geological Society of London 246, 2005).
- Kipf, A. et al. Granitoids and dykes of the Pine Island Bay region, West Antarctica. Antarct. Sci. 24, 473–484 (2012).
- Gallagher, K. Transdimensional inverse thermal history modeling for quantitative thermochronology. *J. Geophys. Res.* 117 https://doi.org/ 10.1029/2011JB008825 (2012).

- Bastías-Silva, J. et al. Uplift and denudation history of the Ellsworth Mountains: insights from low-temperature thermochronology. Solid Earth 15, 555–566 (2024).
- Zundel, M. et al. Thurston Island (West Antarctica) between Gondwana subduction and continental separation: a multistage evolution revealed by apatite thermochronology. *Tectonics* 38, 878–897 (2019).
- Lindow, J. et al. Exhumation history along the eastern Amundsen Sea coast, West Antarctica, revealed by low-temperature thermochronology. *Tectonics* 35, 2239–2257 (2016).
- Carling, P. A. Coevolving edge rounding and shape of glacial erratics: the case of Shap granite, UK. *Earth Surf. Dyn.* 12, 381–397 (2024).
- Golledge, N. R., Fogwill, C. J., Mackintosh, A. N. & Buckley, K. M. Dynamics of the last glacial maximum Antarctic ice-sheet and its response to ocean forcing. *Proc. Natl. Acad. Sci. USA* 109, 16052–16056 (2012).
- Albrecht, T., Winkelmann, R. & Levermann, A. Glacial-cycle simulations of the Antarctic Ice Sheet with the Parallel Ice Sheet Model (PISM) – Part 2: parameter ensemble analysis. *Cryosphere* 14, 633–656 (2020).
- Spiegel, C. et al. Tectonomorphic evolution of Marie Byrd Land implications for Cenozoic rifting activity and onset of West Antarctic glaciation. *Glob. Planet. Change* 145, 98–115 (2016).
- Storey, B. C., Hole, M. J., Pankhurst, R. J., Millar, I. L. & Vennum, W. Middle Jurassic within-plate granites in west Antarctica and their bearing on the break-up of Gondwanaland. *J. Geol. Soc. Lond.* 145, 999–1007 (1988).
- Jordan, T. A. et al. Aerogravity evidence for major crustal thinning under the Pine Island Glacier region (West Antarctica). *Geol. Soc. Am. Bull.* 122, 714–726 (2010).
- Johnson, J. S. et al. Comparing glacial-geological evidence and model simulations of ice sheet change since the last glacial period in the Amundsen Sea Sector of Antarctica. *J. Geophys. Res.* 126, e2020JF005827 (2021).
- Stokes, C. R. et al. On the reconstruction of palaeo-ice sheets: recent advances and future challenges. Quat. Sci. Rev. 125, 15–49 (2015).
- Shepherd, A. et al. Trends in Antarctic Ice sheet elevation and mass. Geophys. Res. Lett. 46, 8174–8183 (2019).
- Prieur, N. C. et al. Automatic characterization of boulders on planetary surfaces from high-resolution satellite images. *J. Geophys. Res.* 128, e2023JE008013 (2023).
- Black, M., Riley, T. R., Ferrier, G., Fleming, A. H. & Fretwell, P. T. Automated lithological mapping using airborne hyperspectral thermal infrared data: a case study from Anchorage Island, Antarctica. *Remote Sens. Environ.* 176, 225–241 (2016).
- Shebl, A. et al. EnMap hyperspectral data in geological investigations: evaluation for lithological and hydrothermal alteration mapping in Neoproterozoic rocks. *Gondwana Res.* 143, 91–124 (2025).
- Adams, J. R. et al. Remote mapping of bedrock for future cosmogenic nuclide exposure dating studies in unvisited areas of Antarctica. *Rem.* Sensing 17, 314 (2025).
- 54. Streickheisen, A. To each plutonic rock its proper name. *Earth Sci. Rev.* **12**, 1–33 (1976).
- Sláma, J. et al. Plešovice zircon A new natural reference material for U-Pb and Hf isotopic microanalysis. *Chem. Geol.* 249, 1–35 (2008).
- Horstwood, M. S. A. et al. Community-derived standards for LA-ICP-MS U-(Th-)Pb geochronology uncertainty propagation, age interpretation and data reporting. *Geostand. Geoanalytical Res.* 40, 311–332 (2016).
- 57. Riley, T., Carter, A. & Johnson, J. S. Geochronological data from the Hudson Mountains, Antarctica (Version 1.0) [Data set]:https://doi.org/10.5285/8f999423-ff40-4181-bdf3-964a7e145772, (2025).
- Vermeesch, P. Statistics for LA-ICP-MS based fission track dating. Chem. Geol. 456, 19–27 (2017).

- McDowell, F. W., McIntosh, W. C. & Farley, K. A. A precise 40Ar–39Ar reference age for the Durango apatite (U–Th)/He and fission-track dating standard. *Chem. Geol.* 214, 249–263 (2005).
- Chew, D. M., Petrus, J. A. & Kamber, B. S. U–Pb LA–ICPMS dating using accessory mineral standards with variable common Pb. *Chem. Geol.* 363, 185–199 (2014).
- Vermeesch, P. IsoplotR: a free and open toolbox for geochronology. Geosci. Front. 9, 1479–1493 (2018).
- Ketcham, R. A., Carter, A., Donelick, R. A., Barbarand, J. & Hurford, A. J. Improved modeling of fission-track annealing in apatite. *Am. Mineral.* 92, 799–810 (2007).
- Gautheron, C., Tassan-Got, L., Barbarand, J. & Pagel, M. Effect of alpha-damage annealing on apatite (U–Th)/He thermochronology. *Chem. Geol.* 266, 157–170 (2009).
- 64. Tinto, K., Bell, R. & Cochran, J. R. *IceBridge Sander AIRGrav L1B Geolocated Free Air Gravity Anomalies, Version 1.* (2010, updated 2019):https://doi.org/10.5067/R1RQ6NRIJV89.
- 65. Jordan, T. & Ferraccioli, F. *Processed line aerogravity data over the Pine Island Glacier basin (2004/05 season)*:https://doi.org/10.5285/E6621111-5965-44DF-B40C-125F466CEB5C, (2020).
- Diehl, T. M. et al. First airborne gravity results over the Thwaites glacier catchment, West Antarctica. Geochem. Geophys. Geosyst. 9, https:// doi.org/10.1029/2007GC001878 (2008).
- von Frese, R. R. B., Hinze, W. J., Braile, L. W. & Luca, A. J. Spherical earth gravity and magnetic anomaly modeling by Gauss- Legendre quadrature integration. *J. Geophys.* 49, 234–242 (1981).
- Pritchard, H. D. et al. Bedmap3 updated ice bed, surface and thickness gridded datasets for Antarctica. Sci. Data 12, 414 (2025).
- 69. Golynsky, A. V. et al. New magnetic anomaly map of the Antarctic. *Geophys. Res. Lett.* **45**, 6437–6449 (2018).
- Talwani, M. & Heirtzler, J. R. in Computers in the mineral industries, Part 1 Vol. 9 464–480 (School of Earth Sciences, Stanford University, 1964).
- Bott, M. H. P. GRAVN (Durham geophysical computer specification, 1969).
- Sanchez, G. et al. PetroChron Antarctica: a geological database for interdisciplinary use. *Geochem. Geophys. Geosyst.* 22, e2021GC010154 (2021).
- Watts, A. B., Xu, C., Searle, M. P., Jurkowski, C. & Shail, R. K. The Permian Cornubian granite batholith, SW England; Part 2: gravity anomalies, structure, and state of isostasy. GSA Bull. 136, 4381–4397 (2024).
- Rignot, E., Mouginot, J. & Scheuchl, B. MEaSUREs InSAR-Based Antarctica Ice Velocity Map, Version 2.:https://doi.org/10.5067/ D7GK8F5J8M8R, (2017).
- 75. Ferraccioli, F. Processed line aeromagnetic data over the Pine Island Glacier basin (2004/05 season) [Data set]:https://doi.org/10.5285/485E6B9B-D033-441F-8C98-B2D0EFCB1D63, (2020).
- Corr, H., Ferraccioli, F. & Vaughan, D. G. Processed airborne radioecho sounding data from the BBAS survey covering the Pine Island Glacier basin, West Antarctica (2004/2005) (Version 1.0) [Data set]:https://doi.org/10.5285/DB8BDBAD-6893-4A77-9D12-A9BCB7325B70, (2021).
- Johnson, J. & Smith, J. Geomorphological measurements and lithological classifications of 90 erratic cobbles from the Hudson Mountains, West Antarctica (Version 1.0) [Data set].:https://doi.org/ 10.5285/79c8eb39-5c19-440e-804f-816cd0b8e4bd, (2024).
- Johnson, J. Orientations of bedrock striations in the Hudson Mountains, West Antarctica (Version 1.0) [Data set]:https://doi.org/10. 5285/7e80c81b-acc2-4a9b-9b5e-d37d49705524, (2024).
- Jordan, T. A., Riley, T. R. & Siddoway, C. S. The geological history and evolution of West Antarctica. *Nat. Rev. Earth Environ.* 1, 117–133 (2020).

Acknowledgements

We thank Hilary Blagbrough, Keir Nichols, Katie Brown, Mark Evans and Dylan Rood for rock sample preparation (cutting, crushing and sieving), Rob Larter, Greg Balco, and John Smellie for discussions that helped formulate the ideas in this paper, and the editor and anonymous reviewers whose comments and suggestions helped improve our paper. Greg Balco kindly prepared Fig. S1. We thank Claus-Dieter Hillenbrand for permission to use photos in Fig. 2. This work is from the 'Geological History Constraints' project, a component of the International Thwaites Glacier Collaboration (ITGC). Support from Natural Environment Research Council (NERC: Grant NE/S006710/1) and the NERC National Capability Single Science (NC): UK Polar Research Expertise for Science and Society: PRESCIENT program. Logistics provided by NSF-U.S. Antarctic Program and NERC-British Antarctic Survey. ITGC Contribution No. ITGC- 153.

Author contributions

T.A.J., J.S.J. and T.R.R. conceived this study together, based on samples and field observations collected by J.S.J. and earlier geophysical work of T.A.J. T.R.R. prepared samples for geochronology and A.C. and E.C. undertook the geochronology analyses and prepared and analysed apatites for thermochronology. T.A.J. modelled the geophysical data. The paper was written collaboratively.

Competing interests

The authors declare no competing interests.

Additional information

Supplementary information The online version contains supplementary material available at https://doi.org/10.1038/s43247-025-02783-3.

Correspondence and requests for materials should be addressed to Tom A. Jordan.

Peer review information *Communications Earth & Environment* thanks Christine Siddoway and the other anonymous reviewer(s) for their contribution to the peer review of this work. Primary Handling Editors: Zhendong Zhang and Alireza Bahadori. A peer review file is available.

Reprints and permissions information is available at http://www.nature.com/reprints

Publisher's note Springer Nature remains neutral with regard to jurisdictional claims in published maps and institutional affiliations.

Open Access This article is licensed under a Creative Commons Attribution 4.0 International License, which permits use, sharing, adaptation, distribution and reproduction in any medium or format, as long as you give appropriate credit to the original author(s) and the source, provide a link to the Creative Commons licence, and indicate if changes were made. The images or other third party material in this article are included in the article's Creative Commons licence, unless indicated otherwise in a credit line to the material. If material is not included in the article's Creative Commons licence and your intended use is not permitted by statutory regulation or exceeds the permitted use, you will need to obtain permission directly from the copyright holder. To view a copy of this licence, visit http://creativecommons.org/licenses/by/4.0/.

© Crown 2025